Available online at www.sciencedirect.com

SciVerse ScienceDirect

Ceramics International 38 (2012) 5949–5956

CERAMICS INTERNATIONAL

www.elsevier.com/locate/ceramint

Effect of Mg doping on photoluminescence of ZnO/MCM-41 nanocomposite

K. Sowri Babu *, A. Ramachandra Reddy, Ch. Sujatha, K. Venugopal Reddy

Department of Physics, National Institute of Technology Warangal, Warangal 506 004, AP, India

Received 20 March 2012; received in revised form 13 April 2012; accepted 14 April 2012
Available online 20 April 2012

Abstract

In this paper, photoluminescence (PL) behavior of $Mg_xZn_{1-x}O$/MCM-41 nanocomposite (where $x = 0.05$, 0.15, 0.25 and 0.30) is reported. Samples were characterized with small angle X-ray diffraction (SAXRD), wide angle XRD, BET (Brunauer–Emmet–Teller) surface area and pore size analyzer, field emission scanning electron microscope (FE-SEM), high resolution transmission electron microscope (HR-TEM) and PL spectrometer. The structure of MCM-41 was confirmed from both SAXRD and BET results. A broad PL band positioned at around 393 nm has been exhibited by ZnO/MCM-41 nanocomposite. With Mg doping, intensity of this PL band decreased for $x = 0.05$ and 0.15 and above this there was gradual enhancement in intensity. It was found that the intensity of the PL band, strongly depends on the particle size of ZnO. The increase in particle size along with MgO phase separation for $x = 0.30$ was proved by HR-TEM analysis. Interestingly, the differences in particle sizes at different concentrations of Mg did not account for shift in the PL band. A twofold enhancement in the intensity of PL band when $x = 0.30$ compared to bare ZnO/MCM-41 nanocomposite was observed. It is attributed for the increase in particle size which preserves the energy saved by passivation of ZnO nanoparticles and the other one is formation of heterojunction structures between ZnO and MgO. It was also evident from these results that there is increase in oxygen vacancies of ZnO crystallites with increase in particle size.

Keywords: B. Nanocomposites; Semiconductors; Mg doped ZnO nanoparticles; Mesoporous silica MCM-41; Photoluminescence

1. Introduction

Zinc oxide (ZnO) is one of the II–VI group binary semiconductors having a wide and direct band gap of 3.37 eV at room temperature and large exciton binding energy of 60 meV. It is one of the important semiconductors that show strong quantum confinement effects in experimentally accessible conditions [1], i.e. variation in optical properties with size. These properties attract a growing attention on ZnO due to its potential applications in short wavelength optoelectronic devices such as UV light emitting diodes (LEDs), laser diodes (LDs) [2–4], and also in solar cells and gas sensors [5]. Most recently, Zeng et al. reported the stable blue luminescence of the ZnO nanoparticles [6]. It may be useful, in visible light emission and also in biological fluorescence labeling applications. Moreover, ZnO is considered as an extremely important material in the field of integrated optics. The fabrication of hybrid organic–inorganic waveguides based on ZnO-(3-glycidoxypropil) trimethoxisilane (GPTS) has also been recently reported by Chiappini et al. [7]. In general, ZnO gives weak and narrow UV emission at around 380 nm and stronger and broader emission band with a maximum between 500 and 530 nm [8]. The suppression of band edge luminescence is due to the fact that smaller nanoparticles possess high surface to volume ratio and therefore larger non radiative paths. To decrease the non-radiative transitions, proper passivation of the surface of the semiconductor nanocrystals is required. The enhancement, in the band edge photoluminescence along with quenching of the green emission of ZnO was obtained when ZnO nanoparticles were incorporated in porous SiO_2 matrix [9]. ZnO/mesoporous silica nanocomposites are important materials that find applications in information storage and optoelectronic devices. The encapsulation of ZnO in mesoporous silica improves the quality of the ZnO nanoparticles surface [9] and reduces the reflection losses in the front surface of optoelectronic devices [10]. Mesoporous silica materials were first discovered

* Corresponding author. Tel.: +91 870 2462593/9849171318; fax: +91 870 2430270.
E-mail address: sowribabuk@gmail.com (K. Sowri Babu).

0272-8842/$36.00
http://dx.doi.org/10.1016/j.ceramint.2012.04.047

by the Mobils research group in the year 1992 and designated these nanoporous molecular sieves as M41S family [11]. MCM-41 (Mobil Catalytic Material number 41) is one member of this family having large surface area (1000 m^2/g) and high pore volume (∼1 cm^3/g). These properties make MCM-41 a good host material especially for semiconductor nanoparticles [12]. The control over the pore size (2–50 nm) and structure (hexagonal, cubic or lamellar phase) of these mesoporous silica materials can be achieved by using different template molecules and concentrations [13].

As mentioned above, ZnO has a potential for various short wavelength optoelectronic device applications. To realize such optoelectronic devices, optical properties of the materials must be engineered controllably. The optical properties of ZnO, can be tuned by doping with suitable transition metals. Among the transition metals, doping of Mg in ZnO is preferred because it may modulate the value of the band gap and increase the UV luminescence intensity. Magnesium oxide (MgO) with a band gap of 7.7 eV has a high transmission in the ultraviolet region [14]. Moreover, Mg^{2+} has ionic radius of 0.57 Å, which is very close to ionic radius of Zn^{2+}, i.e. 0.60 Å. Therefore, replacement of Zn by Mg does not give rise to significant changes in lattice constants. Recent studies demonstrate the enhancement in the band edge luminescence in ZnO doped with MgO [15–17] and a very high intense near band edge luminescence was also reported in ZnO-core/SnO_2-shell nanorods [18]. It is obvious from these results that MgO doping has great influence on visible emission as well as on UV emission of ZnO. Besides this mesoporous MgO–ZnO materials have also been prepared and studied their structural and optical properties [19]. The enhancement in exciton emission and suppression of visible luminescence was observed in $Mg_{0.05}Zn_{0.95}O/SiO_2$ nanocomposite [20]. It has recently been shown that at an appropriate Mg doping of ZnO/SiO_2 nanocomposite, the PL can be tuned by varying excitation wavelength from 475 nm to 635 nm [21]. Moreover, Mg being the lightest material, its addition is expected to reduce the weight of the devices [22]. Therefore, the study of effect of Mg doping on PL of ZnO/MCM-41 is of great significance.

In this work, the synthesis and characterization of $Mg_xZn_{1-x}O$/MCM-41 is reported. HR-TEM analysis reveals the variation in particle size with Mg doping. The intensity variations of the PL band with change of Mg content from $x = 0.05$ to 0.30 are in accordance with the particle size of ZnO. The position of the PL band, did not change with Mg doping. It was found that the intensity of UV emission increased with increase in particle size. The possible mechanisms for the enhancement of PL emission with Mg doping were discussed.

2. Experimental

MCM-41 was prepared by the method reported by Grun et al. [23]. To incorporate ZnO nanoparticles in MCM-41, the method reported by Yang et al. was used [24] with some modifications. Here triethanolamine (TEA) has been used as catalyst and stabilizing agent. The preparation of ZnO/MCM-41 nanocomposite is as follows; one gram of Zn $(NO_3)_2 \cdot 6H_2O$ was dissolved in 50 ml of ethanol and stirred until it becomes clear solution. To this solution, 4 ml of TEA is added and stirred for 1 h and then 0.9 g of MCM-41 was added and stirred for another 0.5 h. Finally, water and ethanol mixture was added. The solution is stirred for 4 h and aged for 24 h. The resultant product was filtered, washed with ethanol several times. After this, sample was calcined at 550 °C in air at a rate of 2 °C/min to obtain ZnO/MCM-41 nanocomposite. To prepare Mg doped ZnO/MCM-41 nanocomposite, Mg and Zn ionic alcoholic solutions were added before MCM-41 mesoporous material was added. The Mg content was varied with $x = 0.05$, 0.15, 0.25 and 0.30.

Small angle X-ray powder diffraction (SAXRD) data were recorded on a Rigaku Ultima-IV diffractometer using Cu Kα (λ = 1.5405 Å) radiation. Wide angle XRD experiments were carried out on Inel-XRG 3000 equipped with Co Kα (λ = 1.7889 Å) radiation. Nitrogen adsorption/desorption isotherms were measured at −196 °C in a Quantachrome NOVA 1200e surface area and pore size analyzer. Morphology of the nanocomposites was studied by using FE-SEM having energy dispersive spectroscopy (EDS) attachment. To get the accurate particle size of ZnO nanoparticles embedded inside the pores of MCM-41, JEOL 3010 high resolution transmission electron microscope (HR-TEM) operating at an accelerating voltage of 200 kV was used. The PL measurements were performed on Jobin Yuon spectrofluorometer, Model: FLUOROLOG - FL3-11 with wavelength resolution of 0.2 nm at room temperature. Xenon arc lamp of 450 W was used as the excitation light source to record the emission spectra of samples.

3. Results and discussion

3.1. Characterization

3.1.1. X-ray diffraction and N_2-sorption studies

The structure of the MCM-41 was studied by BET surface area and pore size analyzer and small angle X-ray diffraction

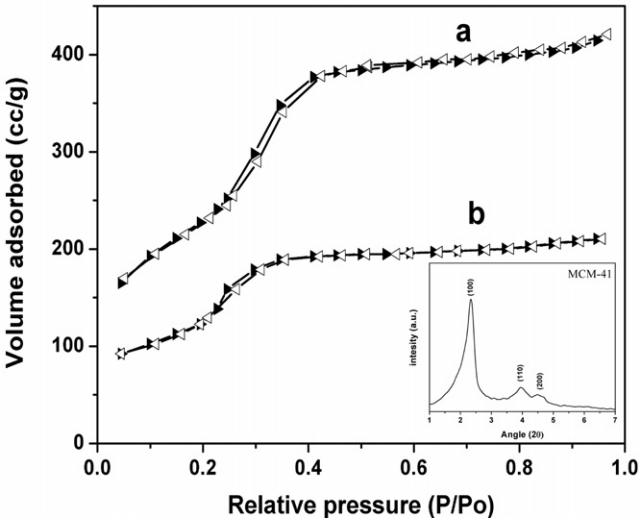

Fig. 1. N_2-adsorption and desorption isotherms of MCM-41 (a) and ZnO/MCM-41 nanocomposite (b) measured at 77 K. Inset: the small angle X-ray diffraction (SAXRD) pattern of MCM-41.

Table 1
BET surface area and pore size analysis results of MCM-41 and ZnO/MCM-41 nanocomposites doped with Mg.

Sample name	Specific surface area (m^2/g)	Total pore volume (cc/g)
MCM-41	952	0.64
ZnO/MCM-41	477	0.29
$Mg_{0.05}Zn_{0.95}O$/MCM-41	484	0.31
$Mg_{0.15}Zn_{0.85}O$/MCM-41	550	0.42
$Mg_{0.25}Zn_{0.75}O$/MCM-41	455	0.35
$Mg_{0.30}Zn_{0.70}O$/MCM-41	402	0.32

(SAXRD) techniques. N_2− adsorption and desorption isotherms of MCM-41 and ZnO/MCM-41 nanocomposite can be seen in Fig. 1. Both samples display type IV-like isotherms according to IUPAC classification. Since the isotherms are same type, it can be concluded that there is no structural collapse of MCM-41 with the incorporation of ZnO nanoparticles in it. The decrease in surface area and pore volume of ZnO/MCM-41 nanocomposite compared to MCM-41 indicates the pore filling process [26]. Table 1 summarizes the surface area and pore volume results obtained from BET. The pore diameter of MCM-41 calculated from the specific surface area and pore volume data comes out to be 2.67 nm which is smaller than pore diameter estimated from SAXRD in the following discussion. The surface area and pore volume of ZnO/MCM-41 nanocomposites was increased up to $x = 0.15$ and decreased thereafter even though composition x was increased further. These changes, observed in the samples, with and without Mg, may be due to the variation of ZnO particle size with Mg doping. Geng et al. reported that there was MgO contribution to the porosity when its concentration was greater than 50% [19]. They reported a surface area of 119.53 m^2/g for mesoporous $(MgO)_{0.75}$–$(ZnO)_{0.25}$ system. Further, according to the Ohtomo et al. formation of MgO phase is ruled out when the concentration of Mg is less than 0.15 [14]. So it can be expected that the increase in surface area and pore volume of Mg doped samples up to $x \leq 0.15$, compared to bare ZnO/MCM-41 nanocomposite could be due to the decrease in particle size. The small angle X-ray diffraction (SAXRD) pattern of MCM-41 was shown in the inset of Fig. 1. which confirmed the structure of MCM-41 and a 3.36 nm-wide effective mean pore diameter can be estimated according to Ref. [23]. Fig. 2 shows the wide angle X-ray diffraction (XRD) patterns of ZnO/MCM-41 nanocomposite and Mg doped ZnO/MCM-41 nanocomposites for Mg contents of $x = 0.15$ and $x = 0.30$. For comparison, XRD pattern of ZnO nanoparticles was also shown in the inset of Fig. 2 which shows the characteristic diffraction peaks of hexagonal ZnO phase (1 0 0), (0 0 2), (1 0 1), (1 0 2), (1 1 0), (1 0 3) and (2 0 0). These characteristic peaks were not detected in nanocomposites but only diffuse peaks of the non-crystalline silica are evident. This implies that ZnO nanoparticles are well incorporated in the pores of MCM-41. So the existence of ZnO in the composite or the MgO phase formation has not been revealed from XRD analysis.

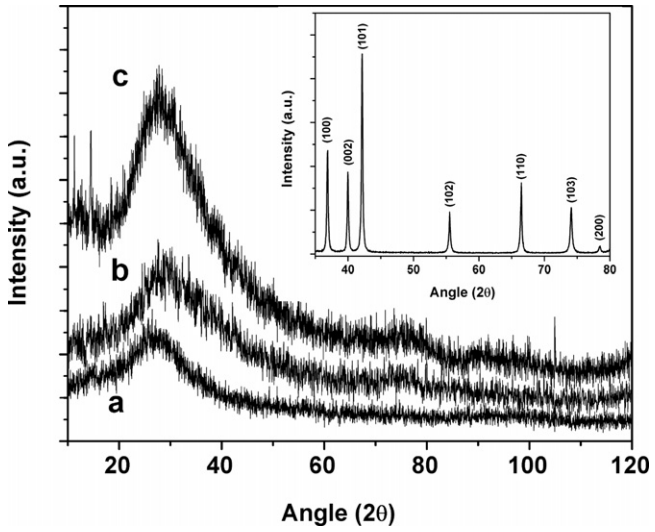

Fig. 2. Wide angle X-ray diffraction (XRD) patterns of ZnO/MCM-41 (a), $Mg_{0.15}Zn_{0.85}O$/MCM-41 (b), $Mg_{0.30}Zn_{0.70}O$/MCM-41 (c) nanocomposites. The inset figure shows the wide angle X-ray diffraction (XRD) pattern of ZnO nanoparticles.

3.1.2. FE-SEM and HR-TEM analysis

The surface morphology and elemental composition was studied by FE-SEM. Fig. 3 shows SEM images of undoped and Mg doped ZnO/MCM-41 nanocomposite. All the nanocomposites exhibited spherical morphology with different particle sizes. It can be seen from these pictures that the particle size decreased with increase of Mg content from $x = 0$ to 0.15 but increased for other compositions. For $x = 0.30$, there is a start of agglomeration of particles which in turn caused changes in the shape of the spherical particles as well (can be seen in Fig. 3(e)). The BET surface area and pore size analyzer results are well supported by these results. For instance, EDS spectrum of $Mg_{0.15}Zn_{0.85}O$/MCM-41 is shown in Fig. 3(f). Further evidence for the existence of ZnO in MCM-41 and variation of particle size with Mg doping was provided by HR-TEM analysis of the nanocomposites. HR-TEM pictures and SAED pattern of $Mg_{0.15}Zn_{0.85}O$/MCM-41 and $Mg_{0.30}Zn_{0.70}O$/MCM-41 are presented in Fig. 4. It can be seen from Fig. 4(a) that Mg doped ZnO nanoparticles are appeared as black dots. The average particle size of the Mg doped ZnO nanoparticles for $x = 0.15$ was calculated to be 2.5 nm and it reached to 15 nm with the increase of Mg content up to 0.30. From the SAED pattern of $Mg_{0.15}Zn_{0.85}O$/MCM-41 nanocomposite, it can be concluded that the ZnO nanoparticles are in amorphous phase. But above $x = 0.15$ there is an increase in particle size and because of the low solid solubility of Mg (4 mol%) in ZnO, there is possibility of formation of MgO phase [14]. The inset of Fig. 4(b) infers that there is a large distribution of particle size. Fig. 4(b) shows clear fringes with spacing of 0.528 nm which is slightly larger than the spacing between the (0 0 0 2) planes in the undoped ZnO crystals. This result exhibits successful doping of Mg ions in ZnO nanoparticles. The (2 0 0) planes of rock salt MgO and intimate contact between ZnO and MgO particles is also evident from this picture. The electron diffraction pattern in Fig. 4(b) demonstrates the polycrystalline

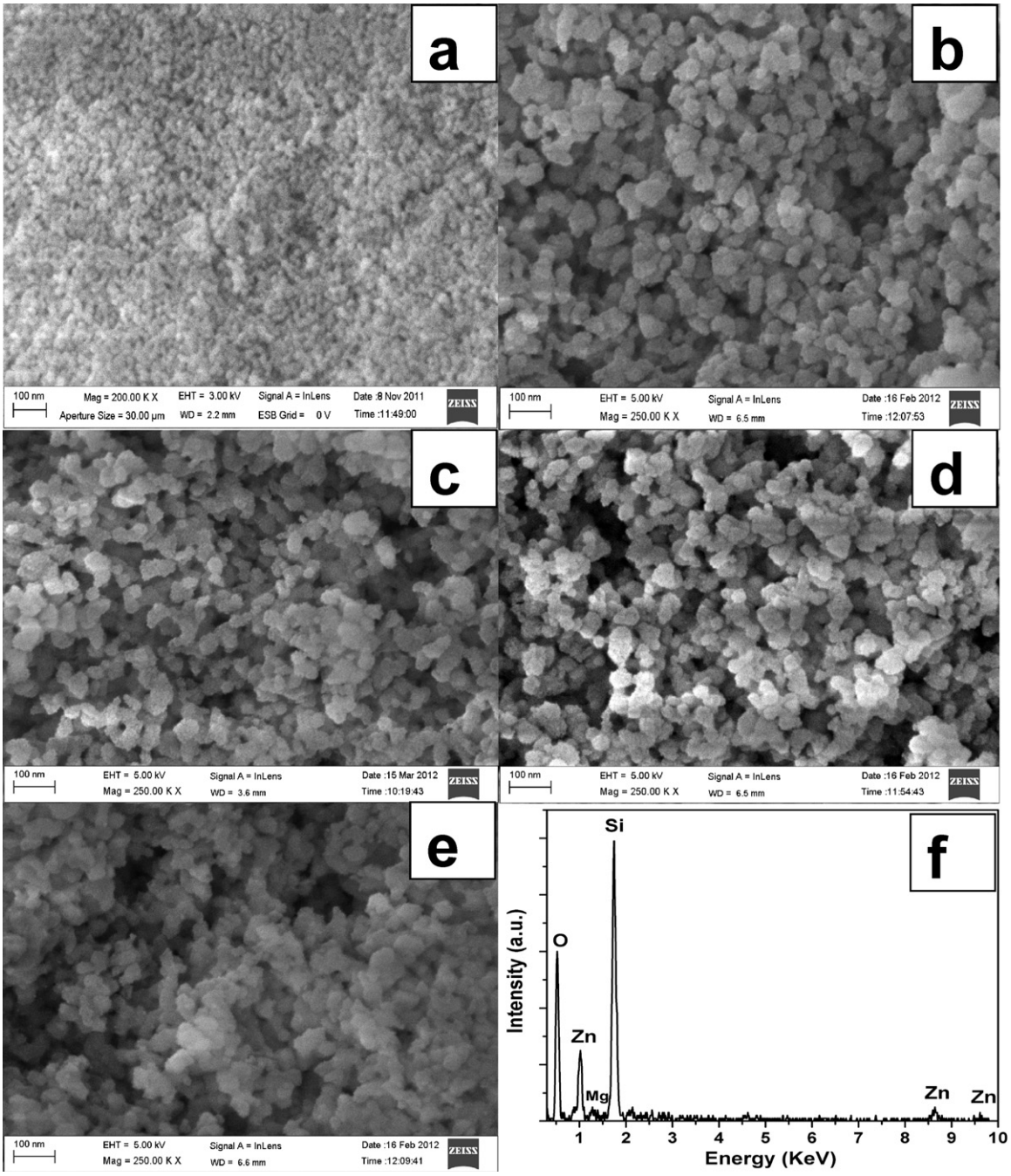

Fig. 3. FE-SEM pictures of ZnO/MCM-41 (a), $Mg_{0.05}Zn_{0.95}O$/MCM-41 (b), $Mg_{0.15}Zn_{0.85}O$/MCM-41 (c), $Mg_{0.25}Zn_{0.75}O$/MCM-41 (d), $Mg_{0.30}Zn_{0.70}O$/MCM-41 (e) nanocomposites and EDS spectrum of $Mg_{0.15}Zn_{0.85}O$/MCM-41 (f) nanocomposite.

nature of ZnO nanoparticles. It can also be seen from these pictures that not all the particles were grown to larger sizes. Electron diffraction (ED) pattern of $Mg_{0.30}Zn_{0.70}O$/MCM-41 was used to analyze the crystalline structure. For that, the *R*-values, the distance between the center spot and the peripheral of different rings in ED patterns, were measured which enables us to calculate the spacing values using the following formula:

$$L\lambda = \mathrm{Rd}$$

where $L\lambda$ is a fixed value for TEM (in this work, 200 kV). Among the six planes indexed in the ED pattern, five (1 0 0), (1 0 1), (1 0 2), (1 1 0), (1 0 3) belongs to the wurtzite structure of ZnO and the remaining one (2 0 0) corresponds to the rock salt structure of MgO.

3.1.3. Photoluminescence study

The PL spectra of ZnO/MCM-41 nanocomposite and Mg doped nanocomposites recorded with an excitation wavelength of 320 nm are shown in Fig. 5. A broad PL band positioned at 393 nm was obtained in the present case is in good agreement with the previous reports [10,12,25,26]. A sharp peak at 568 nm was detected in all these samples. To know the origin of this

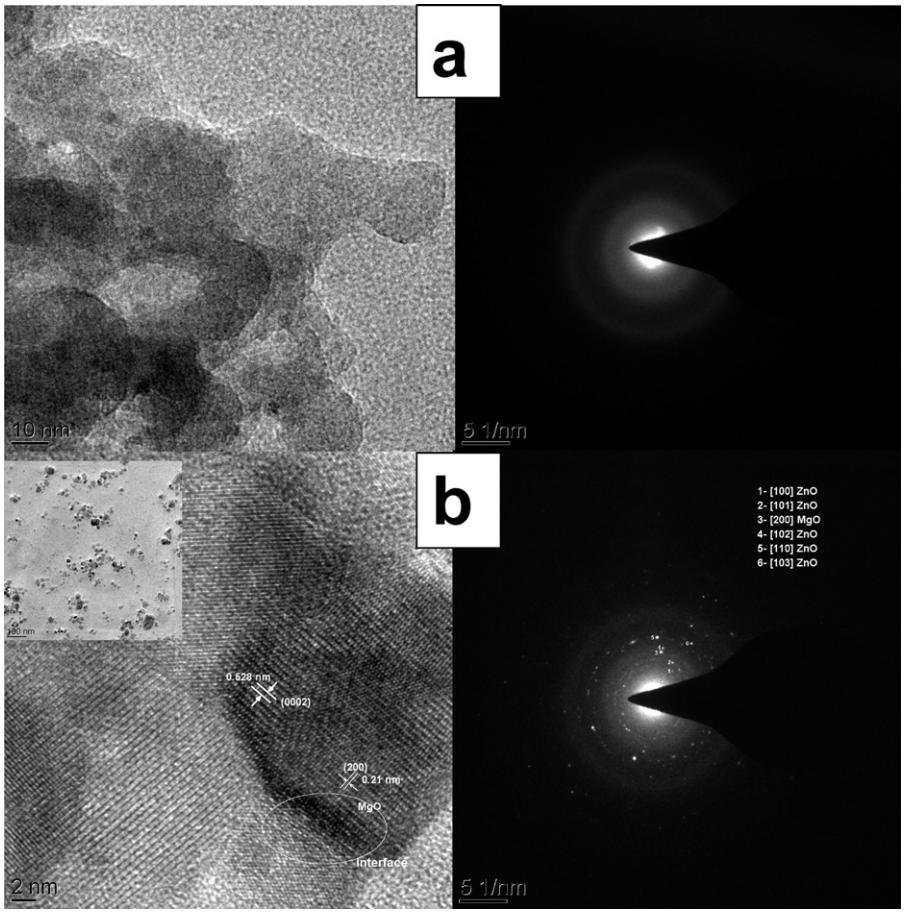

Fig. 4. HR-TEM images and SAED patterns of $Mg_{0.15}Zn_{0.85}O$/MCM-41 (a) and $Mg_{0.30}Zn_{0.70}O$/MCM-41 nanocomposites (b).

peak, the PL spectra of MCM-41 and ZnO were also recorded. In both the samples, this peak was observed and no impurities were detected in the SEM-EDS measurement of samples so it could be due to some measurement error in the instrument which we have used. A small kink, at 363 nm, was observed in almost all samples, which is ascribed to the excitonic emission of ZnO nanocrystals embedded in MCM-41. It has been blue shifted strongly compared to the bulk ZnO whose excitonic emission is at around 380 nm. It confirmed the strong quantum confinement effects of ZnO nanoparticles in the nanocomposite. The position of the excitonic emission was not changed with Mg doping. In fact, the near band edge (NBE) emission shows inverse dependence on the diameter of the particle, such dependence was not observed in this study even though there is variation in particle size with Mg doping. Similar results have also been observed by Karthikeyan et al. recently in Mg doped ZnO nanostructures [27]. It indicates Mg^{2+} addition did not yield any additional energy levels below the conduction band. The generally observed green emission has been quenched completely due to the surface passivation of the ZnO nanocrystals by mesoporous silica host [10,28]. These PL spectra of nanocomposites, doped with different amounts of Mg, exhibited systematic variation in their intensities and particle sizes. The intensity, gradually decreased as the Mg content was changed from $x = 0$ to 0.15 and began to increase for concentrations greater than 0.15. Geng et al. reported the similar kind of variation in NBE emission in mesoporous $(MgO)_x$–$(ZnO)_{1-x}$ system for different x values ($x = 0.05$, 0.25, 0.50 and 0.75). They observed that the NBE emission was decreased for Mg contents 0.05 and 0.25 and enhanced steadily for $x = 0.50$ and 0.70. The decrease in emission intensity for $x = 0.15$, can be explained as follows. As the nanoparticles size decreased, surface/volume ratio was increased and gave rise to larger non-radiative relaxation paths. With large non-radiative relaxation path, the passivation of ZnO nanocrystals does not necessarily lead to the enhancement of the NBE, because the excess energy saved by the passivation is consumed by the non-radiative relaxation path [8,17]. Another reason for the reduction in intensity is that the addition of Mg may inhibit the interactions between ZnO and SiO_2 due to its smaller electro negativity than Zn.

It is evident from BET, FE-SEM and HR-TEM results that the particle size was increased for $x = 0.25$ and 0.30. With increase in particle size, intensity of the PL band enhanced steadily. There is nearly twofold increase in intensity of PL for concentration of Mg doping with $x = 0.30$ compared to the intensity of ZnO/MCM-41 nanocomposite without doping. The deep investigation of PL spectra was done by fitting the curves by three Gaussian functions based on Mahamuni et al. [28] (Table 2). Gaussian fitting results of PL spectra of ZnO/MCM-41 and $Mg_{0.30}Zn_{0.70}O$/MCM-41 nanocomposites are shown in Fig. 5(c) and (d). The PL band of ZnO/MCM-41 nanocomposite showed three emission

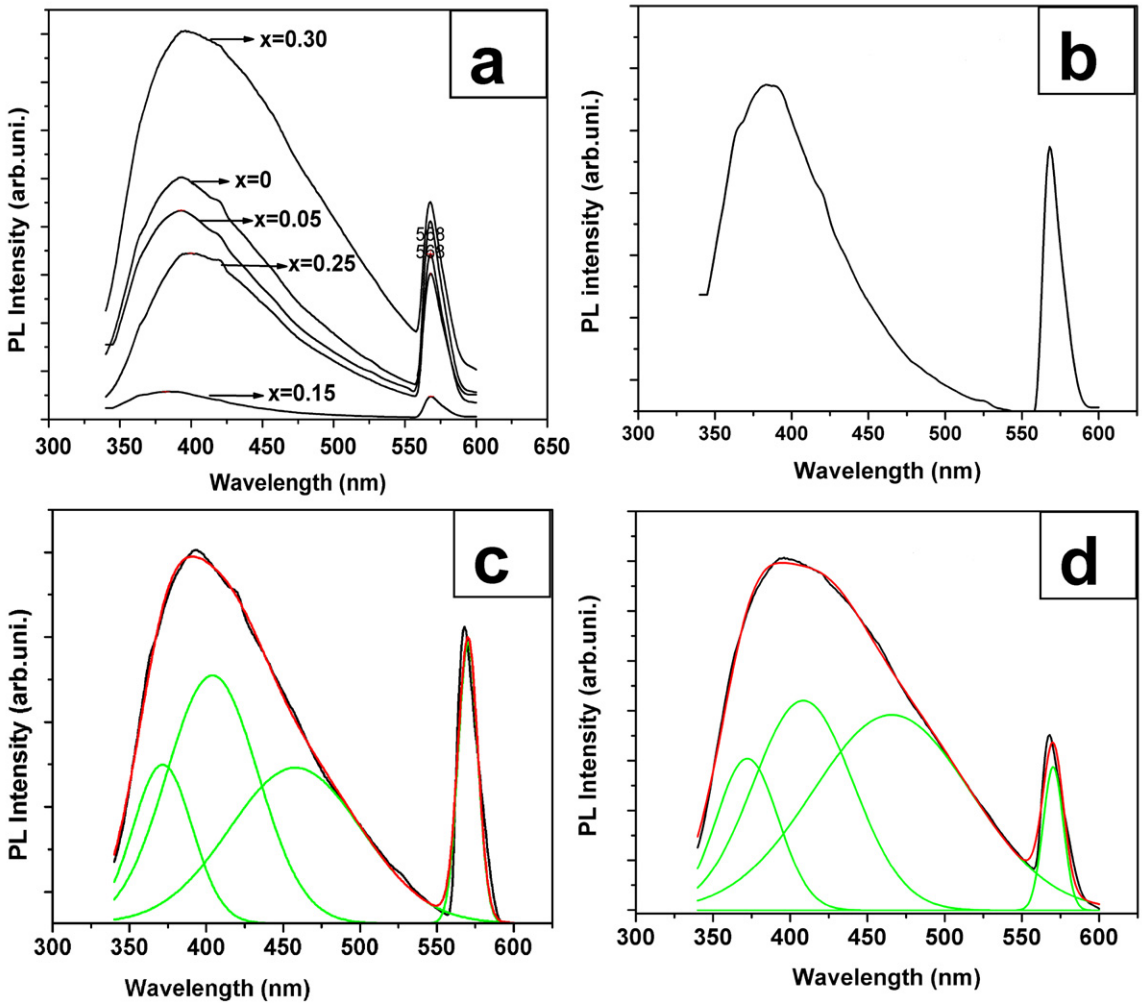

Fig. 5. PL spectra of ZnO/MCM-41 nanocomposite doped with different Mg contents (a), $Mg_{0.15}Zn_{0.85}O$/MCM-41 (b), Gaussian fitted PL spectra of ZnO/MCM-41 (c) and $Mg_{0.30}Zn_{0.70}O$/MCM-41 nanocomposites (d).

peaks situated at 371 nm, 403 nm and 457 nm. These three peaks are attributed to the excitonic emission, oxygen vacancies at the interface between ZnO and SiO_2 and oxygen vacancies in inner ZnO nanocrystals respectively [26,28–30]. From HR-TEM and fitting results of PL, it can be concluded that the FWHM of third peak was increased with increase in particle size which indicates increased oxygen vacancies in inner ZnO crystallites. Here we define intensity ratio between peak 1 and peak 2 as I_1/I_2 and between peak 2 and peak 3 as I_2/I_3. The ratio I_2/I_3 is about six times greater than that observed for ZnO/MCM-41 nanocomposite. It indicates the strong dependence of oxygen vacancies in inner ZnO crystallites on particle size. The formation of MgO when $x = 0.30$ has been confirmed from HR-TEM results. In addition, HR-TEM results also implied that ZnO and MgO particles are in contact intimately. So one of the reasons for increase in intensity of PL band for $x = 0.30$ is increase in particle size. It has also been observed previously in colloidal ZnO nanoparticles [8] and in MgO passivated ZnO nanoparticles [17]. Moreover, with increase of ZnO content in organic–inorganic waveguides, more intense UV emission has been observed [7]. As the particle size increased, the specific surface area decreased as well as the number of charge carriers tunneling from interior to the surface also decreased: as a result, the surface defects were reduced. Consequently, less number of photo-generated carriers will be captured by surface defects and hence there was increase in intensity. However, there may be another phenomenon which can be partly contributed to the enhancement of PL emission which was due to the formation of ZnO/MgO heterojunction structure [16]. The formation of heterojunction structures between ZnO and MgO was confirmed from the HR-TEM analysis. When ZnO/MgO heterojunction structures were formed, charge transfer across the ZnO–MgO boundary took

Table 2
Gaussian fitting results of PL spectra of ZnO/MCM-41 and $Mg_{0.30}Zn_{0.70}O$/MCM-41 nanocomposites.

Sample Name	Peak position	Full width half maximum (eV)	I_1/I_2	I_2/I_3
ZnO/MCM-41	371	32.63	–	–
	403	21.01	0.41	–
	457	14.41	–	0.10
$Mg_{0.30}Zn_{0.70}O$/MCM-41	372	31.00	–	–
	408	19.37	0.44	–
	465	12.15	–	0.67

place which created electron depletion region with width W in the ZnO nanoparticle [31]. Due to this phenomenon, ZnO nanoparticles are electron depleted. So the transition process for non-radiative recombination might be greatly suppressed in the depletion region where the Fermi level dropped below the energy levels due to non radiative transition related defects [31,32]. So the enhancement in PL intensity at high Mg contents can be attributed to the increase in particle size and formation of ZnO/MgO heterojunction structures.

4. Conclusion

In conclusion, the successful incorporation of Mg doping in ZnO nanoparticles, in MCM-41, an inorganic host matrix was achieved. The structure of the composites was analyzed by various techniques such as XRD, BET, FE-SEM, HR-TEM and PL spectrometer. BET, SEM and TEM analysis of samples showed non-linear variation in ZnO nanoparticle size with the addition of Mg. These results demonstrated that the intensity of PL band strongly depended upon particle size. Oxygen vacancies, in inner ZnO crystallites, were enhanced as the particles were grown to larger size. The intensity of PL band was double multiplied for Mg content with $x = 0.30$ compared to the undoped ZnO/MCM-41 nanocomposite. This increase in intensity was attributed to the increase in particle size and also due to the formation of ZnO–MgO heterojunction structures.

Acknowledgments

The authors would like to express thanks to Prof. Sethupathi, Department of Physics, IIT Madras, India for providing the HR-TEM facility. The authors are also thankful to Prof. Bansal, Dean, Department of Physics, University of Hyderabad (UOH), AP, India for permission to use FE-SEM facility. The authors would also like to gratefully acknowledge to Dr. N. Venkatathri, Department of Chemistry, National Institute of Technology, Warangal, for his valuable suggestions.

References

[1] U. Koch, A. Fotik, H. Weller, A. Henglein, Photochemistry of semiconductor colloids. Preparation of extremely small ZnO particles, fluorescence phenomena and size quantization effects, Chemical Physics Letters 122 (1985) 507–510.
[2] R.F. Service, Will UV lasers beat the blues? Science 276 (1997) 895.
[3] A. Hellemans, Laser light from a handful of dust, Science 284 (1999) 24–25.
[4] M.H. Huang, S. Mao, H. Feick, H. Yan, et al., Room-temperature ultraviolet nanowire nanolasers, Science 292 (2001) 1897–1899.
[5] S. Suwanboon, P. Amornpitoksuk, A. Sukolrat, Dependence of optical properties on doping metal, crystallite size and defect concentration of M-doped ZnO nanopowders (M = Al, Mg, Ti), Ceramics International 37 (2011) 1359–1365.
[6] B.H. Zeng, G. Duan, Y. Li, S. Yang, X. Xu, W. Cai, Blue luminescence of ZnO nanoparticles based on non-equilibrium processes: defects origins and emission controls, Advanced Functional Materials 20 (2010) 561–572.
[7] A. Chiappini, C. Armellini, A. Chiasera, M. Ferrari, R. Guider, Y. Jestin, L. Minati, E. Moser, G. Nunzi Conti, S. Pelli, R. Retoux, G.C. Righini, G. Speranza, Preparation and characterization of ZnO particles embedded in organic–inorganic planar waveguide by sol–gel route, Journal of Non-Crystalline Solids 355 (2009) 1132–1135.
[8] A. Van Dijken, E.A. Meulenkamp, D. Vanmaekelbergh, A. Meijerink, The kinetics of radiative and non radiative processes in nanocrystalline ZnO particles upon photoexcitation, Journal of Physical Chemistry B 104 (2000) 1715–1723.
[9] Z. Fu, B. Yang, L. Li, W. Dong, C. Jia, W. Wu, An intense ultraviolet photoluminescence in sol–gel ZnO–SiO_2 nanocomposites, Journal of Physics: Condensed Matter 15 (2003) 2867.
[10] R.J. Martin-Palma, R. Guerrero-Lemus, J.D. Moreno, J.M. Martinez-Duart, Determination of spectral behavior of porous silicon based photodiodes, Solid State Electronics 43 (1999) 1153–1157.
[11] C.T. Kresge, M.E. Leonowicz, W.J. Roth, J.C. Vartuli, J.S. Beck, Ordered mesoporous molecular sieves synthesized by a liquid-crystal template mechanism, Nature 359 (1992) 710–712.
[12] Y. Xiong, L.Z. Zhang, G.Q. Tang, G.L. Zhang, W.J. Chen, ZnO nanoparticles included within all-silica MCM-41: preparation and spectroscopic studies, Journal of Luminescence 110 (2004) 17–22.
[13] L.I. Burova, D.I. Petukhov, A.A. Eliseev, A.V. Lukashin, Yu. D. Tretyakov, Preparation and properties of ZnO nanoparticles in the mesoporous silica matrix, Superlattices and Microstructures 39 (2006) 257–266.
[14] A. Ohtomo, M. Kawasaki, T. Koida, K. Masubuchi, H. Koinuma, Y. Sakurai, T. Yasuda, Y. Segawa, $Mg_xZn_{1-x}O$ as a II–VI wide band gap semiconductor alloy, Applied Physics Letters 72 (1998) 2466–2468.
[15] J. Zhang, F. Pan, W. Hao, T. Wang, Effect of MgO on the luminescent properties of ZnO, Materials Science and Engineering B 129 (2006) 93–95.
[16] Z. Fu, W. Dong, B. Yang, Z. Wang, Y. Yang, H. Yan, S. Zhang, J. Zuo, M. Ma, X. Liu, Effect of MgO on the enhancement of ultraviolet photoluminescence in ZnO, Solid State Communications 138 (2006) 179–183.
[17] S. Yamamoto, T. Mishina, Enhanced band edge photoluminescence from MgO passivated ZnO nanocrystals, Journal of Luminescence 131 (2011) 620–622.
[18] C. Jin, H. Kim, H.Y. Ryu, H.W. Kim, C. Lee, Subwavelength optical resonant cavity – induces enhancement of the near band edge emission from ZnO-core/SnO_2-shell nanorods, Journal of Physical Chemistry C 115 (2011) 8513–8518.
[19] W. Geng, N. Li, X. Li, X. Lai, L. Wang, B. Long, J. Ning, J. Tu, S. Qiu, Synthesis and photoluminescent properties of mesoporous $(MgO)_x(ZnO)_{1-x}$ materials, Materials Research Bulletin 43 (2008) 601–610.
[20] A. Dev, S. Chakrabarti, S. Kar, S. Chaudhuri, Optical properties of $Mg_{0.05}Zn_{0.95}O/SiO_2$ nanocomposite films prepared by sol–gel technique, Journal of Nanoparticle Research 7 (2005) 195–201.
[21] J.H. Hong, Y.F. Wang, G. He, J.X. Wang, Tuning visible emission by choosing excitation wavelength in Mg-doped ZnO/silica composites, Journal of Alloys and Compounds 506 (2010) 1–3.
[22] R. Chandramohan, J. Thirumalai, T.A. Vijayan, S. Valanarasu, S. Elhil Vizhian, M. Srikanth, V. Swaminathan, Nanocrystalline Mg doped ZnO dilute magnetic semiconductor prepared by chemical route, Advanced Science Letters 3 (2010) 319–322.
[23] M. Grun, K.K. Unger, A. Matsumoto, K. Tsutsumi, Novel pathways for the preparation of mesoporous MCM-41 materials: control of porosity and morphology, Microporous and Mesoporous Materials 27 (1999) 207–216.
[24] H. Yang, Y. Deng, C. Du, Synthesis and optical properties of mesoporous MCM-41 containing doped TiO_2 nanoparticles, Colloids and Surfaces A: Physiochemical and Engineering Aspects 339 (2009) 111–117.
[25] H.G. Chen, J.L. Shi, H.R. Chen, J.N. Yan, Y.S. Li, Z.L. Hua, Y. Yang, D.S. Yan, The preparation and photoluminescence properties of ZnO-MCM-41, Optical Materials 25 (2004) 79–84.
[26] W. Zeng, Z. Wang, X.F. Qian, Y. Yin, Z.K. Zhu, ZnO clusters in situ generated inside mesoporous silica, Materials Research Bulletin 41 (2006) 1155–1159.
[27] B. Karthikeyan, T. Pandiyarajan, Simple room temperature synthesis and optical studies on Mg doped ZnO nanostructures, Journal of Luminescence 130 (2010) 2317–2321.
[28] S. Mahamuni, K. Borgohain, B.S. Bendre, Spectroscopic and structural characterization of electrochemically grown ZnO quantum dots, Journal of Applied Physics 85 (1999) 2861–2865.

[29] Shabnam, C.R. Kanth, P. Arun, Controlling the photoluminescence of ZnO:Si nano-composite films by heat-treatment, Materials Research Bulletin 45 (2010) 1368–1374.
[30] B. Yao, H. Shi, H. Bi, L. Zhang, Optical properties of ZnO loaded in mesoporous silica, Journal of Physics: Condensed Matter 12 (2000) 6265–6270.
[31] K. Vanheusden, W.L. Warren, C.H. Seager, D.R. Tallant, J.A. Voigt, B.E. Gnade, Mechanism behind green photoluminescence in ZnO phosphor powders, Journal of Applied Physics 79 (1996) 7983.
[32] X.L. Wu, G.G. Siu, C.L. Fu, H.C. Ong, Photoluminescence and cathodoluminescence studies of stoichiometric and oxygen deficient ZnO films, Applied Physics Letters 78 (2001) 2285.